Spectroscopic Polarizable Force Field for Amide Groups in Polypeptides

Bernhard Schropp, Christoph Wichmann, and Paul Tavan*

Lehrstuhl für Biomolekulare Optik, Ludwig-Maximilians-Universität, Oettingenstrasse 67, 80538 München, Germany

Received: February 12, 2010; Revised Manuscript Received: March 30, 2010

The infrared spectra of polypeptides are dominated by the so-called amide bands. These bands originate from the electrostatically coupled vibrations of the strongly polar amide groups (AGs) making up the polypeptide backbone. Because the AGs are highly polarizable, external electric fields can shift the frequencies of the amide normal modes over wide spectral ranges. The sensitivity to external fields and the strong polarity are the reasons why the shapes of the amide bands can code the structure of the polypeptide backbone. Aiming at a decoding of these band shapes, Schultheis et al. (*J. Phys. Chem. B* **2008**, *112*, 12217) have recently suggested a polarizable molecular mechanics (PMM) force field for AGs, which employs field dependent force constants and enables the computation of the amide bands from molecular dynamics simulations. Here we extend and refine this first suggestion of such a PMM force field. The extension rests on the choice of suitable internal coordinates for the AGs and on the inclusion of the complete AG Hessian and of its field dependence. The force field parameters are calculated from density functional theory. The improved quality of the resulting PMM descriptions is demonstrated using very simple examples and an outlook is given.

1. Introduction

The amide bands dominating the infrared (IR) spectra of proteins and peptides are due to vibrations of the strongly polar and polarizable amide groups (AGs) $C_\alpha-C'O-NH-C_\alpha$ making up the polypeptide backbone.[1−3] Replacing the C_α atoms by methyl groups yields the molecule *N*-methylacetamide (NMA), whose valence structure is depicted in Figure 1. Consequently, NMA represents a minimal model for an AG within a polypeptide.

The most prominent feature of the polypeptide IR spectra is the amide I (AI) band, which belongs to the C′═O stretching motions. Because of dipole−dipole couplings, the corresponding normal modes are delocalized over several AGs. These couplings are steered by the relative orientations and distances of the AGs.[4−6] In addition, the electrostatic field **E**, which is generated by the charged or polar molecular groups present in a peptide−solvent system and which locally acts on a given AG, tunes the normal-mode frequencies of this AG by polarizing its electron density.[7−14] As a result of these effects of electronic polarization, the spectral positions and shapes of the amide bands code the three-dimensional structures of the polypeptides.

As discussed in Schultheis et al.,[7] the derivation of accurate structural information from observed amide bands still poses a major challenge, because a reliable and efficient computational method that can solve this task is not yet available. The basic concepts and ingredients required for the construction of such an approach have been thoroughly discussed in the quoted paper, pointing out that one needs a molecular mechanics (MM) force field for the elastic properties of AGs, in which all parameters depend on the external electric fields. In particular, such a force field will then be capable to capture the structurally sensitive effects of mutual polarization among the AGs, which are caused by their strong electric dipoles and shape the amide bands of proteins and peptides. A corresponding polarizable molecular mechanics (PMM) force field was classified as being of "type II", because conventional (type I) PMM force fields restrict the field dependence to the electrostatic signatures of molecular structures (e.g., through complementing the usual set of fixed atomic partial charges by inducible point dipoles).[15−19]

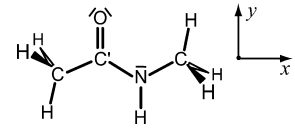

Figure 1. *N*-Methylacetamide (NMA), a minimal model for the AGs in polypeptides. Also indicated is the Cartesian coordinate system used by us for specifying the directions of external fields acting on NMA.

With an accurate PMM/II force field at hand, one will be able to derive the IR spectra of protein and peptide backbones through molecular dynamics (MD) simulations, which sample given conformational states for a few hundreds of picoseconds, and by computing Fourier transforms of time correlation functions (FTTCF; see refs 20 and 21) from the MD trajectories. Alternatively, one may also resort to instantaneous normal-mode analyses of structural ensembles drawn from an MD trajectory.[21] If the polarizability is restricted to the force constants, i.e., if the chosen force field variant does not cover a conventional PMM/I part, the computational cost of PMM/II-MD is essentially identical to that of standard MM-MD simulations. If a PMM/I feature is included, the required self-consistency iteration for the electrostatics increases the computational effort by a factor of about 2, as is common in PMM/I force fields[16] (for a more detailed discussion of the issues of computational cost see ref 7).

A first and quite preliminary version of a PMM/II force field for amide groups was derived from density functional theory (DFT) calculations on the model compound NMA exposed to homogeneous external fields and was implemented into a MD simulation program. We will use the shortcut "PMM/D" for this first version. PMM/D test calculations on the vibrational

* Corresponding author. Phone: +49-89-2180-9220. E-mail: tavan@physik.uni-muenchen.de.

10.1021/jp101358r
Published on Web 04/22/2010

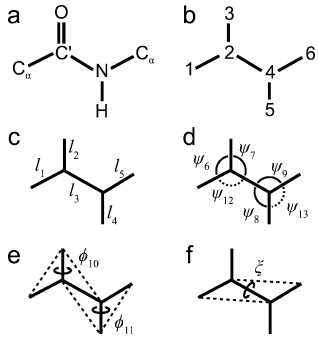

Figure 2. Internal coordinates for our AG force field. (a) Atoms and (b) their numbering. The AG geometry is nonredundantly given by (c) five bond lengths l_i, (d) the first four of the six bond angles ψ_i, (e) two improper dihedral angles ϕ_i, and (f) one proper dihedral angle ξ.

spectra of NMA in the gas phase and in aqueous solution were compared with DFT and DFT/MM results and provided a "proof of principle" for the suggested PMM/II scenario. Furthermore, these comparisons revealed the remaining shortcomings of this first attempt of constructing a PMM/II force field for AGs,[7] some of which will be remedied in this article.

The PMM/D force field for AGs was defined[7] in terms of the nonredundant set $\mathbf{Q} = \mathbf{q} \cup \xi$, $\mathbf{q} \equiv \{q_1, ..., q_{11}\}$, of internal coordinates (ICs) depicted in Figure 2. The AG structure uniquely determines that the five bond lengths l_i, $i \in I_l \equiv \{1, ..., 5\}$, have to be included into $\mathbf{Q}$; i.e., $q_i \equiv l_i$. Four bond angles $q_i \equiv \psi_i$, $i \in I_\psi \equiv \{6, ..., 9\}$, had to be chosen from the six existing candidates. Further below we will show that it is advantageous to additionally include the remaining and redundant bond angles $q_{12} \equiv \psi_{12}$ and $q_{13} \equiv \psi_{13}$, which are marked in Figure 2d by dotted lines, into $\mathbf{Q}$. Furthermore, two so-called improper dihedral angles $q_{10} \equiv \phi_{10}$ and $q_{11} \equiv \phi_{11}$ were employed to describe the locally planar bonding patterns associated with the sp^2 hybridizations of the C′ and N atoms, respectively. Finally, the proper dihedral ξ was selected to model the potential associated with the torsion around the central C′−N bond.

After a well-founded choice[7] of the parameters $\Theta_\xi \equiv \{U_1 = 2.7$ kcal/mol, $U_2 = 12.3$ kcal/mol$\}$, the torsional stiffness of the C′−N bond was expressed by the periodic model potential

$$U_\xi(\xi|\Theta_\xi) = \frac{U_1}{2}[1 + \cos(\xi)] + \frac{U_2}{2}[1 - \cos(2\xi)] \quad (1)$$

which assigns a sizable barrier $\Delta U \approx U_2 + U_1/2$ to the trans−cis isomerization and a higher energy U_1 to the cis ($\xi = 0$) than to the trans state of an AG ($\xi = 180°$). This torsional potential was chosen as independent of the external electric field $\mathbf{E}$ acting on the given AG.[7]

In contrast, a field dependence was assigned to the model potential $U_\mathbf{q}$ for the chemical bonding forces associated with the remaining 11 ICs q_i. As is common in so-called "spectroscopic" force fields[22−24] (the term "spectroscopic" has been introduced in ref 23), this potential $U_\mathbf{q}$ should be given by the quadratic form

$$U_\mathbf{q}[\mathbf{q}|\Theta_\mathbf{q}(\mathbf{E})] = \frac{1}{2}\sum_{i,j=1}^{11} k_{ij}(\mathbf{E})[q_i - q_i^0(\mathbf{E})][q_j - q_j^0(\mathbf{E})] \quad (2)$$

Here, the field dependent parameter set

$$\Theta_\mathbf{q}(\mathbf{E}) = \mathbf{q}^0(\mathbf{E}) \cup \mathbf{K}(\mathbf{E}) \quad (3)$$

consists of the equilibrium values $q_i^0(\mathbf{E})$ of the ICs and of the Hessian matrix $\mathbf{K}(\mathbf{E})$ with the elements

$$k_{ij}(\mathbf{E}) = \left.\frac{\partial^2 U_{qm}(\mathbf{q}, \mathbf{E})}{\partial q_i\, \partial q_j}\right|_{\mathbf{q}=\mathbf{q}^0(\mathbf{E})}, \qquad i, j = 1, ..., 11 \quad (4)$$

which can be calculated from a quantum mechanically determined ground state energy surface $U_{qm}(\mathbf{q}, \mathbf{E})$ of an AG exposed to an external electric field $\mathbf{E}$.

Equations 1−4 complete the description of a PMM/II energy function

$$U[\mathbf{Q}|\Theta_\xi, \Theta_\mathbf{q}(\mathbf{E})] = U_\xi(\xi|\Theta_\xi) + U_\mathbf{q}[\mathbf{q}|\Theta_\mathbf{q}(\mathbf{E})] \quad (5)$$

for an AG as characterized by Figure 2. Such a force field may be chosen as the sum of the nonpolarizable dihedral potential U_ξ for the torsional coordinate ξ and of the field dependent quadratic form $U_\mathbf{q}$ for the remaining ICs $\mathbf{q}$.

In contrast to the PMM/II force field for AGs introduced above, conventional MM force fields such as CHARMM,[25] AMBER,[26] and GROMOS[27] generally neglect the off-diagonal coupling terms k_{ij}, $i \neq j$, characterizing the spectroscopic potential $U_\mathbf{q}$ by the choice $k_{ij} \equiv 0$. Furthermore, such force fields neglect all effects of the electronic polarizability. Thus, they particularly assume that the remaining parameters $\Theta_\mathbf{q}^D \subset \Theta_\mathbf{q}$, which specify the diagonal terms in $U_\mathbf{q}$, are independent of the external electric field.

Adopting the conventional MM concept, also the PMM/D force field[7] for AGs neglected the off-diagonal couplings and solely replaced the parameter set $\Theta_\mathbf{q}^D$ by a field dependent one. This suboptimal choice was motivated by reasons of a most simple first implementation, because PMM/D could be readily integrated into the MD simulation program EGO, which had been originally designed for conventional MM force fields.[28] Thus, this first version of a PMM/II force field for AGs could use the existing code for the computation of chemical bonding forces and, therefore, had to neglect the dynamic couplings k_{ij} among the ICs $q_i \neq q_j$ of an AG.[7]

This neglect was unfortunate, because the choice of the parameters $\Theta_\mathbf{q}$ specifying the model potential $U_\mathbf{q}$ in eq 2 becomes much simpler if one includes the couplings. Then one can simply copy the equilibrium geometry $\mathbf{q}_{qm}^0$ and the associated Hessian matrix $\mathbf{K}_{qm}$ of an AG, which results from a quantum mechanical reference calculation, into $\Theta_\mathbf{q}$. As a result of such a copying procedure, the vibrational spectra and normal modes will be identical to those of the quantum mechanical reference, if the Hessian $\mathbf{K}$ covers all degrees of freedom of the given molecule. In PMM/D, the omission of the off-diagonal terms in $U_\mathbf{q}$ enforced a complicated procedure for computing and optimizing the remaining diagonal force constants k_{ii}. Here, the optimization served to approximately model the effects of the neglected couplings on the normal-mode frequencies of an AG. At the optimal frequency match, however, the PMM/D normal modes showed strong deviations from the quantum mechanical reference results.[7] Therefore it was the first task within this work to include the coupling terms into the potential $U_\mathbf{q}$ and to implement this modified type of potential function into our MD program package EGO.[28]

If one employs a quantum mechanical Hessian $\mathbf{K}_{qm}$ to construct a PMM/II bonding potential $U_\mathbf{q}(\mathbf{E})$, then one has to

analyze its still unknown field dependence. In the case of the PMM/D force field, the field dependence of its parameters had been determined by quantum mechanical calculations on NMA using DFT.[7] Here, the equilibrium geometries $\mathbf{q}^0$ and diagonal force constants k_{ii} were calculated for NMA exposed to homogeneous electric fields $\mathbf{E}$ of varying strengths. These fields were oriented along the axes of the coordinate system shown in Figure 1. As a result, the parameters of linear response functions $\mathbf{q}^0(\mathbf{E})$ and $k_{ii}(\mathbf{E})$ were obtained.[7]

We will generally adopt this DFT based procedure to compute the still unknown response functions $\mathbf{K}(\mathbf{E})$ of the Hessian. We will check for each independent element $\vartheta(\mathbf{E}) \equiv k_{ij}(\mathbf{E}) = k_{ji}(\mathbf{E})$ of the Hessian, whether linear response

$$\vartheta(\mathbf{E}) = \vartheta(0) + \boldsymbol{\alpha}\mathbf{E} \tag{6}$$

holds for field strengths, which are typically encountered in condensed phase environments, as it was the case for PMM/D.[7]

If one assumes a linear response function for all 66 independent force constants $\vartheta(\mathbf{E})$, which are contained in the parameter set $\Theta_{\mathbf{q}}(\mathbf{E})$ characterizing the field dependent bonding potential eq 2, one has to compute by DFT 66 zero-field values $\vartheta(0)$ and as many response parameters $\boldsymbol{\alpha} = (\alpha_x, \alpha_y, \alpha_z)$. Together with the previously computed linear response functions $\mathbf{q}^0(\mathbf{E})$ describing the field dependence of the equilibrium geometry, the potential $U_{\mathbf{q}}$ is thus specified by 308 scalar parameters. The corresponding spectroscopic PMM/II force field for AGs will be called PMM/S. The sheer size of the PMM/S parameter set immediately leads to the question of to what extent it can be reduced without large losses of accuracy. Here we will show that only 40% of the parameters are actually required. All others can be set to zero, leading to a simplified and optimized spectroscopic PMM/II force field for AGs, which we will call PMM/O.

Because AGs are covalently embedded in larger molecular structures, there will be potential energy terms in the total energy function of a corresponding peptide−solvent system that describe the dynamic couplings of the six atoms making up a given AG with all other atoms. Following the usual construction of conventional MM force fields[25−27] these dynamic couplings will cover electrostatic and van der Waals interactions with distant atoms and simple bonding terms with covalently neighboring atoms. Therefore, the vibrations within a given AG will be electrostatically coupled to the vibrations of other AGs, thus automatically accounting for the transition dipole coupling, on which previous approaches were exclusively based.[4−6] On the other hand, the use of conventional "nonspectroscopic" force field terms for the covalent coupling of all those atoms, which are directly attached to the C_α atoms of a given AG (cf. Figure 2a), can introduce certain errors into the vibrational spectra calculated for this AG by PMM/O.

Such errors will already appear when one considers the vibrational spectrum of the NMA molecule depicted in Figure 1, which differs from an AG only through the covalent attachment of six hydrogen atoms to the two C_α atoms. The reason is that all those parts of NMA's complete Hessian, which are associated with motions of the additional hydrogen atoms, derive from a conventional force field,[25] and that only those parts that belong to the ICs of the AG moiety (cf. Figure 2) are exact copies of the quantum mechanical reference Hessian. If one calculates the vibrational spectrum of NMA from such a partially "spectroscopic" energy function, one expects deviations from the quantum mechanical reference spectrum for all those normal modes that contain deformations of the methyl groups.

Nevertheless, we will employ the model compound NMA also in this work as our test system for estimating the quality of our new PMM/O force field for AGs.[7] As a measure we will use comparisons with gas phase and liquid phase spectra calculated by DFT normal-mode analyses and DFT/MM simulations, respectively (as well as comparisons with experimental data).

This article is organized as follows: After a sketch of the employed computational methods, we check the quality at which the PMM/S and PMM/O force fields describe the vibrational spectrum of an AG in the zero-field case. In this context we will explain the various stages of parameter reduction and optimization leading from PMM/S to PMM/O. Next we present the response properties of the force field parameters to external fields and study how well DFT/MM descriptions and experimental mid-IR spectra of protonated and deuterated NMA in D_2O and acetonitrile are reproduced by PMM/O. A short outline of the tasks remaining for further extension and improvement of the method concludes the paper.

2. Methods

Using DFT descriptions of NMA exposed to homogeneous external fields of varying strengths and directions, we have calculated the parameters of the new PMM/S and PMM/O force fields by essentially the same procedures that were previously applied by Schultheis et al.[7] to the parametrization of the first attempt PMM/D of a PMM/II force field. Therefore, a short sketch of these methods suffices here. More detailed explanations are given whenever we use different computational protocols.

As in the previous work,[7] the DFT calculations on NMA were carried out with the program package CPMD[29] employing the so-called MT/BP approach (Becke−Perdew functional,[30,31] Martins−Troullier pseudopotentials,[32] plane wave basis cutoff at 80 Ry, DFT box size of $11.0 \times 10.5 \times 8.0$ Å^3). Homogeneous electric fields were imported into the DFT box using the combination[33] of CPMD with the MM-MD package EGO[28] and the procedures described in ref 34. The fields were oriented along the three axes of the NMA coordinate system shown in Figure 1. Their strengths were chosen as described in section 5.4 of ref 7. In contrast to the previous procedure, however, we have strictly enforced the planarity[35] of the molecule and the mirror symmetry of the methyl hydrogens with respect to the $x-y$-plane by applying suitable constraints.

2.1. PMM/S Parameters for an AG. Using the method described by Palmö et al.,[23] the Cartesian MT/BP Hessians $\mathbf{K}_{\mathrm{qm}}^{\mathrm{NMA}}(\mathbf{E})$ of NMA were transformed to ICs and subsequently projected onto the reduced set $\mathbf{q}$ of ICs characterizing the geometry of a planar AG (cf. Figure 2). Furthermore and as described in more detail in the Supporting Information, we have considered the four possible equilibrium configurations of *trans*-NMA, which are distinguished by the rotameric states of the two methyl groups,[36] and have chosen the Boltzmann-weighted averages $\mathbf{K}_{\mathrm{qm}}^{\mathrm{AG}}(\mathbf{E})$ of the associated projected AG Hessians for further analyses [cf. eq 14 in the Supporting Information].

For each field direction E_u, $u = x, y, z$, we have calculated the configuration average Hessians $\mathbf{K}_{\mathrm{qm}}^{\mathrm{AG}}(\mathbf{E})$ of the AG at 13 field values $E_{u,s} = s\Delta E$ with $s = -6, ..., +6$, and $\Delta E = 5$ kcal/(mol e Å). We have graphically checked at what quality their elements $\vartheta_{\mathrm{qm}}(E_{u,s})$ can be fitted by linear response functions $\vartheta(\mathbf{E})$ as given by eq 6.

This inspection has demonstrated that most elements of the configuration average Hessians obey linear response to a very

good approximation in the chosen range of field strengths (as is demonstrated by the set of figures collected in Sec. 4 of the Supporting Information). Furthermore, this visual analysis has shown that the field-induced deviations

$$\Delta\vartheta_{qm}(E_{u,s}) \equiv \vartheta_{qm}(E_{u,s}) - \vartheta_{qm}(0) \tag{7}$$

of the Hessian matrix elements $\vartheta_{qm}(E_{u,s})$ from the equilibrium values $\vartheta_{qm}(0)$ are either antisymmetric or symmetric functions $\Delta\vartheta(E_u)$ of the field E_u. Accounting for this fact, each of the slopes α_u, $u = x, y, z$, occurring in the linear fit function eq 6 is given by

$$\alpha_u = \begin{cases} \alpha_u^+, & \text{if} \quad \Delta\vartheta(-E_u) = -\Delta\vartheta(E_u) \\ \mathrm{sgn}(E_u)\alpha_u^+, & \text{if} \quad \Delta\vartheta(-E_u) = +\Delta\vartheta(E_u) \end{cases} \tag{8}$$

where α_u^+ is the slope of $\vartheta(E_u)$ at positive fields E_u. The slopes α_u were then determined by linear fits[37] to the deviations $\Delta\vartheta(E_{u,s})$ given by eq 7. Correspondingly, the zero-field value $\vartheta(0)$, which is the second parameter occurring in the linear fit function eq 6, is simply chosen as the element $\vartheta_{qm}(0)$ of the configuration average Hessian $\mathbf{K}_{qm}^{AG}(\mathbf{E})$ at field zero. Note here that our eq 8 corrects an obvious error in eq 7 of ref 7.

As explained in the Introduction, the parametrization of the PMM/S force field is complete as soon as, in addition to the linear response models $\mathbf{K}^{AG}(\mathbf{E})$ for the Hessian of AGs, which we have computed by the above procedures, also the field dependence $\mathbf{q}(\mathbf{E})$ of the AG's geometry is given. Here we have adopted the linear response description specified by Tables 3 and 4 in ref 7.

2.2. Partially Spectroscopic Force Field for NMA. For the MD simulation of NMA in solution the PMM/S force field of its AG must be complemented by bonding potentials modeling the deformations of the two methyl groups, whose attachment transforms an AG into NMA. Adopting once again a corresponding suggestion from ref 7, here we used a simplified CHARMM22 force field.[38] Furthermore, the electrostatic and van der Waals interactions with other molecules in a simulation system must be parametrized. Here, our choice differs from the earlier one. Whereas in ref 7 the methyl hydrogen atoms carried no Lennard-Jones potentials, we now included the potentials prescribed by CHARMM22. Similarly, instead of using uncharged methyl groups we now computed partial charges from the 78.6 ps hybrid (MT/BP)/MM-MD trajectory of NMA in TIP4P water[39] at 300 K and ambient pressure presented and discussed in ref 7. This trajectory contains the so-called ESP (electrostatic potential) partial charges[33,40] of all NMA atoms at each integration step, because these charges are used to compute the electrostatic action of the DFT fragment NMA on the surrounding MM solvent. Averaging these ESP charges over the trajectory for each atom of NMA and additionally over all hydrogen atoms of a given methyl group yields the partial charges listed in Table 1. These average liquid phase ESP charges were used in all our MD simulations on NMA in water. Concerning the electrostatic interactions of NMA with the surrounding aqueous solvent, they can guarantee an optimal match—in a mean field sense—of PMM/S-MD results with the DFT/MM-MD reference data.

Despite its extension by CHARMM22 ingredients and by DFT/MM liquid phase partial charges, we use the name "PMM/S" of the AG force field also for the thus-obtained NMA force field. Note here that in PMM/S the electrostatic signature of the AG has been chosen as nonpolarizable quite like in its predecessor PMM/D.

TABLE 1: Partial Charges q_i for NMA

i[a]	atom	q_i/e
	$H_m(C')$	0.135
1	$C_\alpha(C')$	−0.466
2	C'	0.758
3	O	−0.781
4	N	−0.504
5	H	0.354
6	$C_\alpha(N)$	0.183
	$H_m(N)$	0.017

[a] Atom numbers i as defined in Figure 2b for an AG.

2.3. Vibrations of the AG within NMA. We have selected NMA as our test molecule, because it differs from an AG within a polypeptide chain solely at the methyl groups. As explained above, we have chosen a most simple model for the methyl groups, because we are not particularly interested in the methyl deformations in NMA and want to determine a force field for AGs instead. Unfortunately, however, many of NMA's amide modes are strongly coupled to methyl deformations.[41−43] To compute the vibrational spectra of the AG within NMA without being bothered too much by the methyl groups, we reduce the masses $m(H_m)$ of the methyl hydrogens by a factor of 10^{-5} (cf. ref 7). Within normal-mode analysis,[44] the methyl deformations are then strongly blue-shifted and largely decoupled from the amide modes. Thus, the frequencies and normal modes of the AG within NMA were obtained by such a normal-mode analysis.

2.4. Optimization of PMM/S. The AG spectra thus obtained by DFT will still be influenced by couplings of the methyl deformations with the C_α (C')−C' and N−C_α (N) elongations l_1 and l_5, respectively. Because these couplings are ignored in the PMM/S description of NMA, the copying of the associated entries k_{11} and k_{55} from the MT/BP Hessian $\mathbf{K}_{qm}^{AG}(0)$ into the PMM/S energy function will lead to differences between the AG spectra calculated by PMM/S and MT/BP.

We will check to what extent an empirical variation of k_{11} and k_{55} can make these differences small. Furthermore, using comparisons of the MT/BP and PMM/II spectra calculated by normal-mode analyses for the AG within NMA, we will systematically investigate which of the matrix elements in the Hessian $\mathbf{K}_{qm}^{AG}(0)$ can be omitted without changing the frequencies and mode compositions of the amide bands (in the given zero-field case) too much. These analyses will lead to the optimized AG force field PMM/O.

2.5. MD Simulations of NMA in Solution. To compute the IR spectra from FTTCF, we carried out PMM/O-MD simulations of protonated and deuterated NMA in aqueous solution. Here, as in ref 7, a periodic rhombic dodecahedron with an inner radius R_i of 19 Å was filled with a single NMA model and with 1403 deuterated water models described by Jorgensen's transferable four-point potential[39] (TIP4P). Furthermore, we generated a simulation system for protonated NMA surrounded by 946 acetonitrile models[45] ($R_i = 24.5$ Å). The systems were equilibrated for several nanoseconds in the *NpT* ensemble using a Berendsen thermostat[46] (coupling time 0.5 ps, target temperature 293 K) and barostat[46] (coupling time 5 ps, target pressure 1×10^5 Pa). The electrostatics were treated by toroidal boundary conditions,[28] which include a moving-boundary reaction field description for electrostatic interactions at distances larger than R_i and fast hierarchical multipole expansions up to the quad-

rupole moment.[47,48] For the dielectric constant of the distant continuum we chose 78 (water) and 37.5 (acetonitrile). The equations of motion were integrated with the Verlet algorithm[49] at a time step of 0.2 fs. During the initial equilibration the NMA model was chosen nonpolarizable.

Subsequently, we switched on the PMM/O force field for NMA, decoupled this solute molecule from the Berendsen thermostat thus realizing a noninvasive control of its temperature,[50] and turned off the barostat. After 50 ps equilibrations we performed 105 ps production runs. The field dependence of the force field parameters [cf. eq 6] was treated as described in ref 7. Exceptions are that all nonbonded interactions within the AG of NMA were neglected and that the field at the hydrogen atom was omitted in the computation of the average field $\mathbf{E}_{pol}$ polarizing the core of the AG. Thus $\mathbf{E}_{pol}$ was evaluated as $(\mathbf{E}_O + \mathbf{E}_{C'} + \mathbf{E}_N)/3$ from the fields at the atoms O, C′, and N of an AG.

The IR spectra of NMA in solution were calculated by FTTCF[21] from the MD trajectories of NMA's dipole moment (covering 2^{19} time steps). Then they were scaled with the harmonic approximation quantum correction factor[51] and noise was reduced by convolution with a Gaussian kernel of 5 cm^{-1} standard deviation. The bands in the FTTCF spectra were assigned by instantaneous normal-mode analyses following the procedures described in ref 21. The positions $\tilde{\nu}_i$, widths σ_i, and intensities P_i of the bands were determined by fitting models

$$S(\tilde{\nu}) = \sum_{i=0}^{n} P_i \exp(-(\tilde{\nu} - \tilde{\nu}_i)^2/(2\sigma_i^2))$$

consisting of n Gaussian distributions to the FTTCF spectra. Here, for the spectral regions covered by the FTTCF spectra, the numbers n of Gaussians were derived from the instantaneous normal-mode analyses.

3. Results

We will first address the spectral effects of including the nondiagonal couplings in the zero-field AG force field PMM/S defined by eq 2. Subsequently we will consider the pruning and optimization leading to the energy function PMM/O.

3.1. Force Field of an Isolated AG. The second column of Figure 3 shows the vibrational frequencies of an isolated AG obtained with our new spectroscopic force field PMM/S. The first (PMM/D) and last (MT/BP) columns of the figure repeat earlier results on the vibrational spectrum of an AG applying this time, however, scale factors, which were proposed for comparisons with experimental spectra.[7]

By comparing the first two columns in Figure 3, one sees that including the coupling terms in the force field substantially shifts the frequencies of all in-plane vibrational levels (solid lines) toward the MT/BP reference frequencies. Whereas for PMM/D the root-mean-square deviation (rmsd) from the MT/BP frequencies is 91 cm^{-1}, it is reduced to 22 cm^{-1} for PMM/S. Moreover, also the normal-mode vectors $\mathbf{a}_i$, i = I, ..., VI, predicted by PMM/S are much closer to those of the reference calculation ($\mathbf{b}_i$) than the vectors calculated with PMM/D. As a measure we compute the average scalar products $S = (1/6)\sum_i \mathbf{a}_i \cdot \mathbf{b}_i$ of the (normalized) normal-mode vectors and obtain the values $S = 0.949$ and $S = 0.996$ for PMM/D and PMM/S, respectively. Thus, the PMM/S result almost reaches the target value $S = 1.0$, which signifies perfectly matching modes.

The sizable rmsd of 22 cm^{-1} remaining for the frequencies predicted with PMM/S is mainly due to the AIV mode (cf. Figure 3). Here, PMM/S overestimates the reference frequency by 46 cm^{-1}. The AIV mode is characterized by the coupled stretches of the $C_\alpha(C')-C'$ and $N-C_\alpha(N)$ bonds. Particularly for these stretches deviations had to be expected, because PMM/S, in contrast to MT/BP, neglects the couplings with the deformations of the methyl groups which, in NMA, are localized at the two C_α atoms (cf. section 2.4). This observation has led us to the idea that the associated stretching force constants k_{11} and k_{55} should be considered as free parameters in the subsequent optimization and simplification of the force field PMM/S.

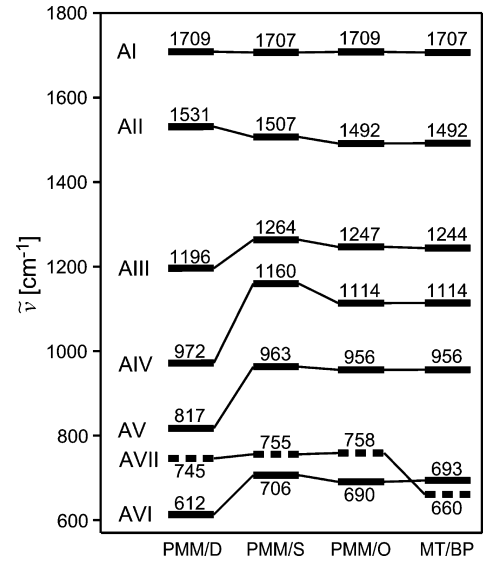

Figure 3. Vibrational frequencies of an "isolated AG" obtained with different force fields (see section 2.3 for the methods to generate these spectra by normal-mode analysis[44] and by a decoupling of the hydrogen motions). PMM/D, first version of a PMM/II force field;[7] PMM/S, spectroscopic force field eq 2; PMM/O, pruned and optimized energy function; MT/BP, DFT reference. The PMM/D spectra are scaled by the factor 0.9925 and the other spectra are scaled by 1.0354.[7] Solid lines mark in-plane modes; dashed lines mark out-of-plane modes. The compositions of the PMM/D and MT/BP modes are characterized in Figure 7 of ref 7.

Although we did not yet explain the detailed steps leading to the optimized force field PMM/O, Figure 3 already shows in column three the result of this endeavor. After optimization all the shown frequencies of the in-plane AG modes closely match the reference values, bringing the rmsd down to 2 cm^{-1}. Furthermore, the excellent match with the reference normal modes is retained as is witnessed by the value $S = 0.998$ of the average scalar product. The high quality at which the normal-mode analysis of an AG with PMM/O reproduces the MT/BP result clearly justifies the notion "spectroscopic" for the optimized force field.

3.2. Pruning and Optimization of PMM/S. The spectroscopic AG force field PMM/S is specified by a rather large parameter set. To reduce the number of these parameters, we have analyzed the configuration averaged Hessian $\mathbf{K}_{qm}^{AG}(\mathbf{E})$, which is defined in eq 14 of the Supporting Information, for an isolated AG, i.e., for $\mathbf{E} = 0$.

According to eq 4 this (11×11) matrix also refers to the improper dihedral angles ϕ_{10} and ϕ_{11} defined in Figure 2. However, by symmetry these two out-of-plane coordinates do not couple with the remaining in-plane coordinates q_i, $i \in I_{ip} \equiv I_l \cup I_\psi$. Furthermore, the zero-field coupling term $k_{10,11}$ obtained by MT/BP for ϕ_{10} and ϕ_{11} turned out to be very small. Therefore, we decided to describe the two

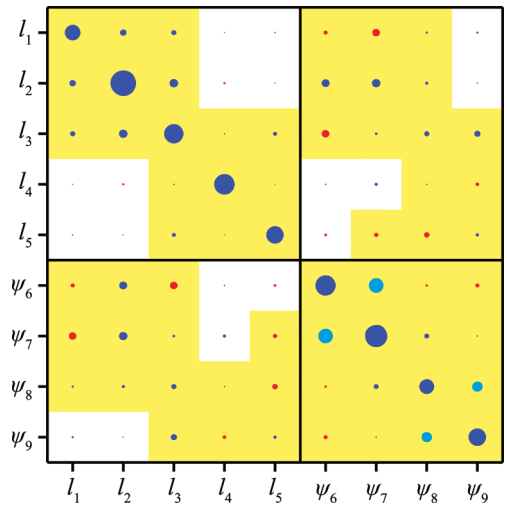

Figure 4. Conformation average Hessian matrix $\mathbf{K}_{qm}^{AG}(0)$ of an AG, which is defined in the Supporting Information. It was obtained by MT/BP, and is restricted to the nine in-plane ICs q_i characterized in Figure 2. The area of a dot measures the absolute value of the associated matrix element. Blue dots mark positive values, red dots mark negative values, and cyan dots mark positive coupling terms that are replaced by a redundant harmonic potential. White background indicates neglected matrix elements.

improper dihedrals with two decoupled ($\tilde{k}_{10,11} = \tilde{k}_{11,10} = 0$) harmonic potentials, i.e.

$$\tilde{U}_{\phi}(\phi_{10}, \phi_{11}|\mathbf{E} = 0) = \sum_{i=10}^{11} \frac{\tilde{k}_{ii}(0)}{2}(\phi_i - 180°)^2 \qquad (9)$$

where the force constants $\tilde{k}_{ii}(0)$, $i = 10, 11$, were copied from the associated diagonal elements $k_{ii}(0)$ of the configuration average MT/BP Hessian $\mathbf{K}_{qm}^{AG}(0)$.

Figure 4 graphically represents the (9×9) Hessian $\mathbf{K}_{qm}^{AG}(0)$ obtained by MT/BP calculations for the remaining nine in-plane ICs q_i, $i \in I_{ip}$. Here, the upper left square belongs to the five stretching coordinates l_i, $i \in I_l$, and the lower right square belongs to the four nonredundant bond angles ψ_i, $i \in I_\psi$. The upper right and lower left rectangles represent the couplings between the stretches and the angle deformations.

An inspection of Figure 4 demonstrates that all dots drawn on a white background in Figure 4 are very small. Neglecting any of the corresponding nine independent off-diagonal matrix elements $k_{ij} = k_{ji}$ increased the rmsd of the AG spectrum from the MT/BP spectrum by less than 0.5 cm^{-1}. If we denote the force constants entering PMM/O by $\tilde{k}_{ij}$, we thus chose $\tilde{k}_{ij} = 0$ at $(ij) \in J_1 \cup J_2$, with the sets of index pairs $J_1 = \{(14), (15), (24), (25)\}$ and $J_2 = \{(19), (29), (46), (47), (56)\}$. The neglected matrix elements k_{ij} describe small couplings between the distant bond stretches $[(ij) \in J_1]$ and small couplings between distant stretches and bond angles $[(ij) \in J_2]$.

The largest couplings between ICs are marked in Figure 4 by cyan dots. These dots refer to the couplings of the bond angles ψ_i and ψ_{i+1}, $i = 6, 8$, which are centered at each of the two sp^2 hybridized atoms (C′ or N, see Figure 2). Our subsequent investigations on the field dependence of the Hessian $\mathbf{K}_{qm}^{AG}(\mathbf{E})$, whose results will be discussed further below, have shown that much more stable linear response relations are obtained, if one replaces for such angles ψ_i and ψ_{i+1} the coupled energy function eq 2 by a new purely harmonic energy function. This function then contains as additional variables the respective dependent bond angles $\psi_{12} = 360° - (\psi_6 + \psi_7)$ and $\psi_{13} = 360° - (\psi_8 + \psi_9)$, which are marked in Figure 2 by dotted lines. Thus we replace, e.g., for the angles ψ_6 and ψ_7 the contribution

$$U(\psi_6, \psi_7) = \frac{1}{2}\sum_{i,j=6}^{7} k_{ij}(\psi_i - \psi_i^0)(\psi_j - \psi_j^0) \qquad (10)$$

to the original PMM/S force field by the purely harmonic contribution

$$\tilde{U}(\psi_6, \psi_7, \psi_{12}) = \frac{1}{2}\sum_{i \in \{6,7,12\}} \tilde{k}_{ii}(\psi_i - \psi_i^0)^2 \qquad (11)$$

to the force field PMM/O. This new contribution is specified by the force constants

$$\tilde{k}_{66} = k_{66} - k_{67}, \qquad \tilde{k}_{67} = 0,$$
$$\tilde{k}_{77} = k_{77} - k_{67}, \qquad \tilde{k}_{12,12} = k_{67} \qquad (12)$$

Thus, the large positive coupling constant k_{67}, which is visible as one of the cyan dots in Figure 4, now appears as the harmonic force constant of the redundant angle ψ_{12}. Furthermore, the direct coupling between the angles ψ_6 and ψ_7 is removed and the PMM/S diagonal force constants (k_{66}, k_{77}) are sizably reduced in PMM/O. Copying the transition from eq 10 to eq 11, also the PMM/S terms $U(\psi_8, \psi_9)$ are replaced by a harmonic PMM/O contribution $\tilde{U}(\psi_8, \psi_9, \psi_{13})$. The Supporting Information contains the proof that such replacements leave the energy function invariant, if the new force constants $\tilde{k}_{ij}$ are given by eq 12 in terms of the original entries k_{ij} of the MT/BP Hessian [cf. eqs 15−17 in the Supporting Information].

After the above simplification and reformulation of the PMM/S force field, we finally arrive at PMM/O by considering the diagonal force constants $\tilde{k}_{11}$ and $\tilde{k}_{55}$ associated with the bond stretches l_1 and l_5, respectively, as free parameters. Monitoring the rmsd in a grid search revealed that the best frequency match is obtained at the values $\tilde{k}_{11} = 0.94k_{11}$ and $\tilde{k}_{55} = 0.92k_{55}$, which are here given in terms of the original PMM/S force constants. Thus, in PMM/O the bond stretches l_1 and l_5 become a little softer, which explains the red shift of the AIV mode in the transition to PMM/O (cf. Figure 3).

3.3. Field Dependence. Having determined a reduced set of force constants $\tilde{k}_{ij}(0)$ for the energy function PMM/O at zero field, we now will prune the field dependent parameter set $\Theta_q(\mathbf{E})$ defined by eq 3. Here, we first set all those force constants to zero, i.e., $\tilde{k}_{ij}(\mathbf{E}) = 0$, which were neglected in the zero-field case (white background in Figure 4).

Next, we calculate linear response functions $\tilde{k}_{ij}(E_u)$ [cf. eq 6], $u \in \{x, y, z\}$, for all nonzero force constants $\tilde{k}_{ij}$ by applying the fit procedures described in section 2.1 to an ensemble of MT/BP Hessians $\mathbf{K}_{qm}^{AG}(E_u)$, which were obtained for NMA exposed to external fields E_u of varying strengths and directions (data not shown). The linear fits are characterized by the zero-field values $\tilde{k}_{ij}(0)$ and by constants $\alpha_{ij,u}$.

As explained in section 2, we enforced symmetry and planarity when exposing NMA to external fields in our MT/BP calculations. As a result of this constraint, all force constants associated with in-plane ICs became independent of fields E_z perpendicular to the molecular plane shown in Figure 1. Thus, the associated response parameters vanish, i.e., $\alpha_{ij,z} = 0$, $i, j \in$

TABLE 2: Diagonal PMM/O Force Constants $\tilde{k}_{ii}(0)$ and Response Parameters $[\alpha_{ii,u}/\tilde{k}_{ii}(0)]^a$

i	q_i	$\tilde{k}_{ii}(0)$	$\alpha_{ii,x}/\tilde{k}_{ii}(0)$	$\alpha_{ii,y}/\tilde{k}_{ii}(0)$
1	l_1	547[b]	−4.10	−1.57
2	l_2	1582[b]	−0.827	5.64
3	l_3	898[b]	5.62	−3.50
4	l_4	1009[b]	−0.141[d]	0.736
5	l_5	673[b]	−3.49	−0.856
6	ψ_6	4.07[c]	−2.85[d]	−0.434
7	ψ_7	5.81[c]	−12.7	1.33[d]
8	ψ_8	2.30[c]	1.11	−2.57
9	ψ_9	4.13[c]	−13.2	5.99
12	ψ_{12}	4.38[c]	6.37	−0.417
13	ψ_{13}	2.16[c]	2.40	−2.68

[a] In [(kmol Å e)/kcal]. [b] In [kcal/(mol Å^2)]. [c] In [kcal/{mol (10 deg)^2}]. [d] Parameters ϑ with $\Delta\vartheta(-E_u) = \Delta\vartheta(E_u)$.

I_{ip}. Because neither the symmetry nor the planarity of NMA had been enforced in the earlier MT/BP calculations leading to the force field PMM/D,[7] these calculations suggested nonzero dependencies on fields $E_z \neq 0$. However, a close analysis (skipped here) has shown that these dependencies are computational artifacts.

Table 2 lists the thus obtained nonzero parameters of the response functions $\tilde{k}_{ii}(\mathbf{E})$ for the in-plane and diagonal part of the quadratic contribution

$$\tilde{U}_{\mathbf{q}}[\mathbf{q}|\tilde{\Theta}_{\mathbf{q}}(\mathbf{E})] = \frac{1}{2}\sum_{i,j=1}^{9}\tilde{k}_{ij}(\mathbf{E})[q_i - q_i^0(\mathbf{E})][q_j - q_j^0(\mathbf{E})] + \frac{1}{2}\sum_{i=10}^{13}\tilde{k}_{ii}(\mathbf{E})[q_i - q_i^0(\mathbf{E})]^2 \quad (13)$$

to the AG force field. The associated coupling functions $\tilde{k}_{ij}(\mathbf{E})$, $i, j \in I_{ip}$, $i \neq j$, are given by the parameters in Table 3 (see the Appendix). The response functions $\tilde{k}_{ii}(\mathbf{E})$ for $i = 10, 11$, which describe the field dependence of the out-of-plane part of $\tilde{U}_{\mathbf{q}}$ and are omitted from Table 2, will be addressed separately below. The description of the AG force field PMM/O is complete, when one adds to the function $\tilde{U}_{\mathbf{q}}[\mathbf{q}|\tilde{\Theta}_{\mathbf{q}}(\mathbf{E})]$ specified by eq 13 the torsional potential $U_{\xi}(\xi|\Theta_{\xi})$ defined by eq 1, thus replacing in eq 5 the PMM/S term $U_{\mathbf{q}}[\mathbf{q}|\Theta_{\mathbf{q}}(\mathbf{E})]$ [cf. eq 2] by the PMM/O term $\tilde{U}_{\mathbf{q}}[\mathbf{q}|\tilde{\Theta}_{\mathbf{q}}(\mathbf{E})]$.

Most interesting among the data listed in Table 2 are the diagonal force constants $\tilde{k}_{22}(0)$ and $\tilde{k}_{33}(0)$ together with the associated response parameters $\alpha_{22,y}$ and $\alpha_{33,y}$, because they belong to the C′═O and C′−N stretches dominating the important AI and AII modes (cf. Figure 7 in ref 7) of the AGs. The y-components $\alpha_{ii,y}$ of the linear response parameters $\boldsymbol{\alpha}_{ii}$ are of key interest here, because the average reaction field $\langle\mathbf{E}\rangle_{liq}$, which is generated by a polar liquid surrounding a solvated and dipolar AG, is directed into the negative y-direction. The field $\langle\mathbf{E}\rangle_{liq}$ has been calculated by us from the 78.6 ps DFT/MM trajectory of a NMA molecule in water described in ref 7. By averaging over the trajectory and over the fields at the atoms O, C′, and N we obtained $\langle\mathbf{E}\rangle_{liq} \approx -34\mathbf{e}_y$ kcal/(mol e Å), where $\mathbf{e}_y$ is the unit vector pointing into the y-direction of the molecular frame depicted in Figure 1.

As is demonstrated by a corresponding comparison, the PMM/O values of $\tilde{k}_{22}(0)$ and $\tilde{k}_{33}(0)$ in Table 2 are by about 10% and 20% larger than the corresponding PMM/D values in Table 3 of ref 7. Nevertheless, because of the included couplings, unscaled PMM/O predicts smaller AI and AII frequencies than unscaled PMM/D (cf. Figure 3). Table 3 in the Appendix reveals, e.g., that the constant $\tilde{k}_{23}(0)$ coupling the C′═O and C′−N stretches is quite large and is much larger than all other stretch−stretch couplings.

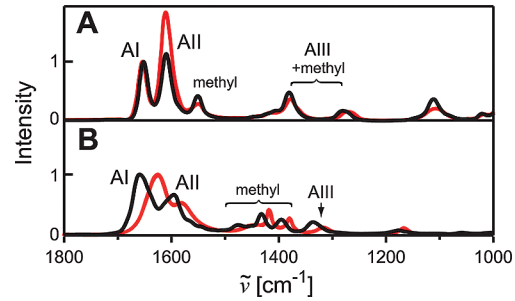

Figure 5. FTTCF spectra of NMA in TIP4P water obtained with two different PMM/II force fields (A) compared with DFT/MM-MD results[7] and experimental data[43] (B). (A) Black curve, PMM/O[c] with its mean field geometry $\tilde{\mathbf{q}}^{0,c}$; red curve, PMM/O extended by a field dependent[7] equilibrium geometry $\mathbf{q}^0(\mathbf{E})$. (B) Black curve, DFT/MM result from ref 7; red curve, experimental IR spectrum of NMA in water taken from ref 43. Intensities are normalized to those of the AI bands.

Although the important response parameters $\alpha_{22,y}$ and $\alpha_{33,y}$ determined for PMM/O quantitatively differ from their PMM/D counterparts (Table 4, ref 7), they show qualitatively the same behavior. When exposed to $\langle\mathbf{E}\rangle_{liq}$, the C′═O stretch gets much softer and the C′−N stretch much stiffer for both force fields (cf. also Figure 8 in ref 7). Note that also the couplings vary strongly upon transfer from the gas phase into the liquid. For $\tilde{k}_{23}$, e.g., this variation is about 10%.

For the remaining parameters of the AG force field, which cover the out-of-plane degrees of freedom (ϕ_{10}, ϕ_{11}) and the equilibrium values $\mathbf{q}^0$ of all ICs $\mathbf{q}$, we decided to use a mean-field approach instead of an explicit field dependence. As we will show now, this choice, which strongly reduces the set of force field parameters, does not affect the frequencies of the in-plane amide bands very much.

3.4. Mean Field Approximation for $\mathbf{q}^0$. Tables 3 and 4 of ref 7 list the parameters of linear response relations $\mathbf{q}^0(\mathbf{E})$ for the equilibrium geometry of an AG. Furthermore and as mentioned above, the average reaction field $\langle\mathbf{E}\rangle_{liq}$ acting on the AG of NMA in liquid water has a strength of about 34 kcal/(mol e Å). Inserting this field into the quoted linear response relations yields the mean field estimate $\tilde{\mathbf{q}}^{0,c} \equiv \mathbf{q}^0(\langle\mathbf{E}\rangle_{liq})$ for the AG geometry. If one assumes that the average reaction fields in polar condensed phase environments are of similar magnitude and direction, the geometry $\tilde{\mathbf{q}}^{0,c}$ should be applicable also to AGs in solvated proteins and peptides. Table 4 of the Supporting Information lists and compares $\tilde{\mathbf{q}}^{0,c}$ with the gas phase geometry $\tilde{\mathbf{q}}^{0,g} \equiv \mathbf{q}^0(\mathbf{E} = 0)$ obtained[7] from the MT/BP description of isolated NMA.

The two equilibrium geometries $\tilde{\mathbf{q}}^{0,g}$ and $\tilde{\mathbf{q}}^{0,c}$ distinguish two different versions of our PMM/O force field for AGs, namely the gas phase force field PMM/O^g and the condensed phase force field PMM/O^c. The AG frequencies displayed in Figure 3 were obtained with the gas phase version PMM/O^g, of course. If one applies PMM/O^c to the isolated NMA molecule, the AG frequencies hardly change. The results of the two normal-mode analyses differ by a rmsd of only 2 cm^{-1}. Thus, it seems that field dependent changes $\mathbf{q}^0(\mathbf{E})$ of the equilibrium geometry can safely be neglected in PMM/II computations of AG vibrational spectra.

This conclusion is further supported by Figure 5. Parts A and B of the figure compare IR spectra of NMA in water calculated by FTTCF from 105 ps PMM/II-MD trajectories (top,

see section 2.5 for technical details) with earlier DFT/MM results[7] and experimental data[43] (bottom). The black spectrum in Figure 5A results from our condensed phase force field PMM/O^c, which applies the mean field approximation to the equilibrium geometry. The red spectrum was obtained by combining PMM/O with the field dependent geometry $\mathbf{q}^0(\mathbf{E})$ suggested in ref 7.

Considering the band positions within the two spectra displayed by Figure 5A, we note an excellent match. The relative intensity of the AII band represents the only marked difference between the predictions of the two force fields. PMM/O^c assigns nearly equal intensities to the AI and AII bands. In contrast, including a field dependent equilibrium geometry $\tilde{\mathbf{q}}^0(\mathbf{E})$ leads to the prediction that the AII band carries a much larger intensity than AI. The latter prediction is far off, because the DFT/MM reference simulation[7] (black curve in Figure 5B) and the experimental IR spectrum of NMA in water[43] (red curve in Figure 5B) both show that the intensity of the AI band should be larger than that of AII. Thus, in this respect the spectrum predicted by PMM/O^c (Figure 5A, black) models the DFT/MM reference (Figure 5B, black) much better than the spectrum obtained with a field dependent geometry. This seemingly counterintuitive result may be due to the larger algorithmic noise that is associated with a field dependent equilibrium geometry $\tilde{\mathbf{q}}^0(\mathbf{E})$ (see further below).

On the other hand, there are still several notable differences between the PMM/O^c prediction of NMA's solution spectrum and the DFT/MM reference result, which have several different causes. For instance, PMM/O^c still overestimates the relative intensity of the AII band. This error is caused by the neglect of a subtle coupling between the charge distribution within the AG and its geometry. The inclusion of geometry dependent partial charges can remove this error, as we intend to show in a subsequent study. Other deviations between the PMM/O^c model and the DFT/MM reference are due to NMA's methyl groups, whose PMM/O^c description represents a strong oversimplification (cf. section 2.3). Nevertheless, i.e., despite the crude methyl model, PMM/O^c can predict the solution frequencies of NMA's amide bands quite well, as we will show in more detail further below. At this point of our presentation, the above comparison mainly served us to demonstrate that the inclusion of field dependent equilibrium geometries into PMM/II force fields represents an unnecessary complication.

Moreover, such an inclusion leads to a strongly increased algorithmic noise, which can modify the temperature of AG groups during MD simulations. For instance, in the PMM/O^c-MD simulation, from which the black spectrum in Figure 5A was extracted, the temperature of the NMA molecule was at 291 K and, thus, by 50 K smaller than in the PMM/O-MD simulation with a field dependent geometry $\tilde{\mathbf{q}}^0(\mathbf{E})$, which produced the red spectrum. Recall that in our MD simulations NMA was always excluded from the thermostat that kept the solvent temperature at 293 K in both cases. We are not sure whether the intensity differences apparent between the black (PMM/O^c) and red (PMM/O) spectra in Figure 5A are caused by the different temperatures of the NMA solute. Note, however, that we intend to show in a subsequent study how energy conservation can be guaranteed when using PMM/II force fields thus generating an algorithm lacking any algorithmic noise.

3.5. Mean Field Approximation for $\tilde{U}_\phi$. As mentioned further above, we also applied a mean field approximation to the harmonic force field contribution $\tilde{U}_\phi(\mathbf{E})$ given by eq 9. This contribution belongs to the improper dihedral angles ϕ_{10} and ϕ_{11} (cf. Figure 2) and describes the stiffnesses of the sp^2 hybridizations at the AG atoms C′ and N.

The choice of mean field values $\tilde{k}_{ii} \equiv k_{ii}(\langle\mathbf{E}\rangle_{liq})$, $i = 10, 11$, for the force constants in $\tilde{U}_\phi(\mathbf{E})$ was motivated by the fact that the associated out-of-plane modes do not couple with the important in-plane amide modes. At the average field $\langle\mathbf{E}\rangle_{liq}$ acting in the liquid on NMA's AG, the force constant $\tilde{k}_{11,11} = 2.31$ kcal/[mol (10 deg)^2] is 2 times larger than its zero-field counterpart[7] $k_{11,11}(0)$, which indicates that the sp^2 hybridization of atom N is strongly enhanced in the liquid. The other force constant $\tilde{k}_{10,10} = 7.04$ kcal/[mol (10 deg)^2] is essentially the same as in the zero-field case, pointing toward an sp^2 hybridization of atom C′ that hardly depends on the environment. Note that we used field dependent force constants $k_{ii}(\mathbf{E})$ with response functions adopted from ref 7 in the PMM/II simulation with the field dependent equilibrium geometry $\tilde{\mathbf{q}}^0(\mathbf{E})$ (red spectrum in Figure 5A) and mean field values in the PMM/O^c simulations (black spectrum in Figure 5A). No frequency differences of bands below 1200 cm^{-1} are visible, which proves the high quality of the mean field approach for the harmonic force constants $\tilde{k}_{ii}$ belonging to the improper dihedrals.

With the choice of mean field parameters for the equilibrium geometry $\tilde{\mathbf{q}}^c$ and for the force field contribution $\tilde{U}_\phi$, we have completed the definition of our new spectroscopic force field PMM/O^c for AGs in condensed phase environments. Due to the pruning of the force constant matrix and due to the use of a mean field approach for many parameters, the originally 308 parameters required for PMM/S are now reduced to 119 nonvanishing PMM/O^c parameters without sacrificing accuracy. To characterize the properties of PMM/O^c, we finally consider NMA in solvents of different polarities.

3.6. NMA Spectra in Different Solvents. Based on the PMM/O^c-MD simulations and FTTCF procedures described in section 2.5, we first consider the resulting IR spectra of NMA and of its N−D isotopomer in water, because for this solvent experimental spectra,[43,52] DFT/MM reference data, and preliminary PMM/II results[7] are available for comparison. These comparisons are presented in Figure 6, parts A (N−H) and B (N−D). The frequencies, which are given here as results of different theoretical methods, were obtained by fitting mixtures of Gaussian bands to the corresponding FTTCF spectra (cf. section 2.5).

According to Figure 6, for both isotopomers of NMA the frequencies of the amide bands predicted by PMM/O^c are much closer to the DFT/MM references than the frequencies obtained by the simple PMM/D description. Overall, the PMM/O^c predictions deviate from the references by an rmsd of only 13 cm^{-1}, whereas for PMM/D the deviation is 64 cm^{-1}. Therefore, the PMM/O^c results describe the experimental amide frequencies at a quality similar to that of the much more expensive DFT/MM-MD approach. The improvements delivered by the transition from PMM/D to PMM/O^c are particularly impressive for the AIII (N−H) and AII′ (N−D) bands. If one disregards the accidental splitting of the AIII band predicted by PMM/O^c (cf. Figure 6A), which is caused by a coupling of the AIII mode with a necessarily ill-described methyl deformation, and calculates the average AIII frequency, one misses the DFT/MM reference result by only 1 cm^{-1}. In contrast, PMM/D underestimates the reference result by as much as 117 cm^{-1}. As is demonstrated by Figure 6B, PMM/D overestimates the reference frequency of the upper AII′ band by 92 cm^{-1} (without any interference of one of the methyl deformations). PMM/O^c, in

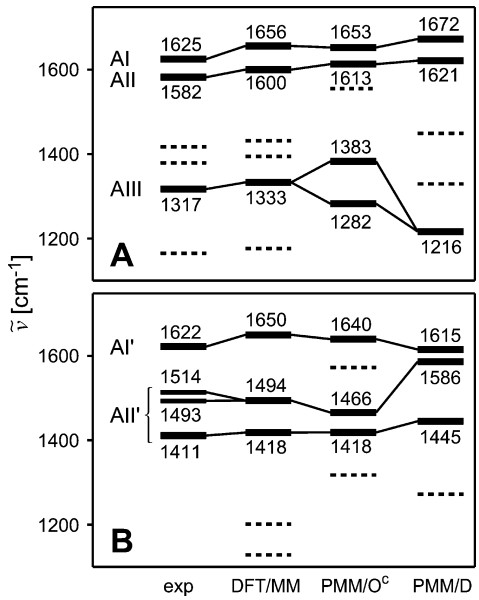

Figure 6. Vibrational frequencies of NMA (A) and of its N−D isotopomer (B) in liquid water. The plots compare IR data[43,52] ("exp") with earlier DFT/MM and PMM/D results,[7] and with our new PMM/O^c description. The DFT/MM and PMM/O^c frequencies are scaled by 1.0354; the PMM/D frequencies are scaled by 0.9925. Bold lines mark amide modes; dashed lines mark methyl modes.

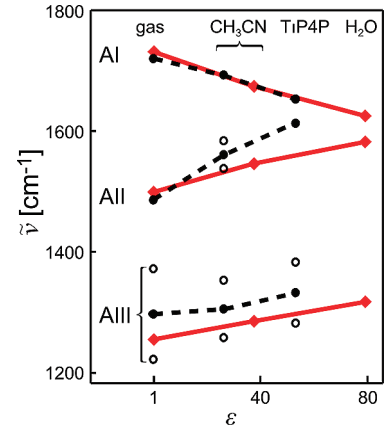

Figure 7. Dependence of NMA's amide band frequencies on the dielectric constant ε of the solvent. The red diamonds and solid lines show experimental data.[43] The black dots and dashed lines mark our PMM/O^c results. The frequencies of calculated amide bands, which are split by coupling to methyl modes (open circles), are represented by the respective average values.

contrast and despite an artificial coupling with a higher frequency methyl mode, underestimates the reference by only 28 cm^{-1}.

Thus, our optimized spectroscopic force field PMM/O does not only reproduce the spectral locations of the amide bands, which are predicted by the parent DFT approach for an isolated amide group, much better than PMM/D (cf. Figure 3), but can also cover the solvatochromic shifts upon transfer into an aqueous solution at a much higher quality. For a detailed investigation of such shifts it would have been desirable, if—in addition to the costly DFT/MM simulations of NMA in water—also DFT/MM simulations of NMA in solvents of different polarities would have been available as further references. We did not attempt to generate such data, because of the huge computational cost demanded by DFT/MM calculations, and because the IR spectrum of NMA is known for an additional solvent, i.e., for acetonitrile (CH_3—C≡N). This fact extends the possibility of judging the performance of PMM/O^c concerning the description of solvatochromic shifts toward another solvent by direct comparison of PMM/O^c results with IR data.

In such a comparison one can then account for the fact that simulation models of liquids may have dielectric constants differing from those of the real liquids. For instance, the TIP4P model potential has a dielectric constant $\varepsilon = 53$ and, thus, is somewhat less polar than liquid water at the same conditions ($\varepsilon = 78$).[17,53] Similarly, the acetonitrile model used by us[45] in a PMM/O^c-MD simulation aiming at NMA's solution spectrum (cf. section 2.5) has a dielectric constant $\varepsilon = 26$, whereas the real liquid is more polar with $\varepsilon = 37$.

Figure 7 compares the frequencies of NMA's AI, AII, and AIII bands observed by IR in environments of different polarities (red) with corresponding PMM/O^c predictions (black) by plotting these frequencies as functions $\tilde{\nu}(\varepsilon)$ of the solvent's dielectric constant. Because the computed AII and AIII bands occasionally turned out to be split due to mixing with nearby (and ill-described) methyl deformations, we took in these cases the average frequencies as measures for the spectral locations of the associated uncoupled amide modes.

The experimental frequencies of the AI bands are seen to decrease linearly with the dielectric constant of NMA's environment (topmost red line). In contrast, the observed AII and AIII frequencies increase with ε though likewise in a nearly linear fashion (other red lines). For the AI band, the PMM/O^c description of the solvatochromic frequency shift (topmost black dashed line) closely matches the IR data. For the AII and AIII bands, however, the simulation results on $\tilde{\nu}(\varepsilon)$ slightly differ from these data. In the case of AIII one notes a general 30 cm^{-1} overestimate of the IR frequency. For AII the predicted frequency just fits for the isolated NMA molecule, but is predicted to be more strongly blue shifted in polar media than observed by IR.

The above comparison leads to the conclusion that the PMM/O^c model for NMA's response to reaction fields in polar solvents is reasonable but not yet perfect. A perfect match would have been a surprise, because NMA's response properties were derived from assuming the external fields to be homogeneous while reaction fields generated by condensed phase environments are actually inhomogeneous. For water molecules embedded in a liquid aqueous environment, e.g., we have recently shown by DFT/MM calculations that the polarizing reaction field, which is the average field over the volume occupied by the given water molecule, is by 30% smaller than the field acting locally at the position of the oxygen atom. Thus, the field $\mathbf{E}_{pol}$ polarizing the AG of NMA will also be some volume average, which most probably differs from our preliminary estimate $\mathbf{E}_{pol} = (\mathbf{E}_O + \mathbf{E}_{C'} + \mathbf{E}_N)/3$ (cf. section 2.5). Consequently, a more precise estimate as to how one should compute $\mathbf{E}_{pol}$ from the local fields at the atoms is required as one of the subsequent tasks.

4. Summary and Discussion

With their original suggestion of a PMM/II force field (called PMM/D by us) for the computation of amide spectra, Schultheis et al.[7] have solely provided a motivation and a proof of principle that the PMM/II approach is capable of describing the important solvatochromic shifts of amide bands. With the first follow-up study presented above we moved a major step toward the proof of practice.

First, we have shown that the inclusion of couplings among the ICs into the AG force field leads to a nearly perfect reproduction of the DFT reference spectra for the isolated AG. Next we have demonstrated that the 308 parameters, by which such a spectroscopic PMM/II force field is originally characterized, can be replaced without loss of accuracy by a much smaller set comprising only 119 elements. In this process of force field pruning and optimization we showed that one may safely choose the geometry of an AG as independent of the polarizing field, and we calculated mean field values for the geometric parameters from a DFT/MM-MD simulation. Furthermore, we demonstrated that instead of including couplings between bond angles at a given central atom one may equally well choose a redundant set of angles at that atom. Note that the latter procedure is common practice in conventional MM force fields such as CHARMM.[25]

The resulting pruned and optimized force field PMM/O^c turned out to reproduce the DFT/MM reference spectra of NMA's N−H and N−D isotopomers in aqueous solution much better than PMM/D. In addition, the PMM/O^c description of the observed IR spectra was seen to be quite close to the very accurate DFT/MM reference. By comparing the experimental IR data on the AI, AII, and AIII frequencies of NMA in different environments[43] with PMM/O^c simulation results, we finally demonstrated that the PMM/O^c description of solvatochromic shifts is reasonable. On the other hand, it is not yet perfect most likely because of our preliminary guess on how to evaluate the polarizing field in condensed phase environments.

The above results represent a major step toward a PMM/II force field, which finally will enable the accurate computation of protein and peptide amide spectra. Nevertheless, a few further steps must be taken until this goal is reached.

(i) In the current formulation, the field dependence $k_{ij}(\mathbf{E})$ of the force constants (weakly) violates the conservation of the total energy. However, a fully Hamiltonian formulation is feasible and it remains to be shown that such an extension does not reduce the quality of spectra computation.

(ii) Up to now the partial charges of the AGs were chosen independent of the geometry. However, the well-known resonance structures of AGs (cf. e.g., ref 7) suggest that such a dependence should exist. Preliminary results then indicate that the inclusion of this effect brings the PMM/O^c intensities close to the DFT/MM reference values.

(iii) Furthermore, the partial charges were chosen independent of the external field. This assumption should be abandoned in favor of a fluctuating charge model.[7,54]

(iv) Polarizable models require knowledge about the size and structure of field inhomogeneities in typical condensed phase environments to enable accurate measurements of the polarizing field.

(v) Finally the "through-bond" coupling of two covalently bound AGs remains to be scrutinized. Such studies will have to answer the question to what extent the 1−3 exclusion of electrostatic interactions commonly assumed in MM force fields like CHARMM[25] can be adopted into a PMM/II modeling of the protein backbone.[7] Note here that one better leaves the conventional 1−3 exclusion of van der Waals interactions unchanged.

Work on all these tasks is in progress.

Acknowledgment. This work was supported by the Deutsche Forschungsgemeinschaft (Grant TA116/8-1, Beschreibung der Amid-Schwingungsbanden von Polypeptiden: Weiterentwicklung und Validierung eines neuen Rechenverfahrens).

TABLE 3: Off-Diagonal PMM/O Force Constants $\tilde{k}_{ij}(0)$, $i \neq j$, and Response Parameters $[\alpha_{ij,u}/\tilde{k}_{ij}(0)]$[a]

i	j	$\tilde{k}_{ij}(0)$	$\alpha_{ij,x}/\tilde{k}_{ij}(0)$	$\alpha_{ij,y}/\tilde{k}_{ij}(0)$
		Stretch−Stretch		
1	2	94.5[b]	8.54	3.86
1	3	57.0[b]	9.17	−1.62[c]
2	3	168[b]	−4.95	2.82
3	4	3.19[b]	25.1[c]	−34.6
3	5	34.5[b]	−12.5	−1.53
4	5	1.74[b]	94.1	−46.5
		Bend−Bend		
6	8	−0.108[d]	21.4	−23.9
6	9	−0.321[d]	−53.1	−18.4
7	8	0.451[d]	−7.84	8.85
7	9	−0.0382[d]	767	−222
		Stretch−Bend		
1	6	−3.43[e]	−14.7	−15.6
1	7	−12.5[e]	−8.57	3.33[c]
1	8	0.875[e]	3.59[c]	2.19
2	6	13.1[e]	13.4	6.19
2	7	15.1[e]	−6.51	5.85
2	8	1.90[e]	−10.9	1.38
3	6	−12.7[e]	−5.37[c]	−0.617
3	7	1.37[e]	−187	59.0
3	8	5.38[e]	9.83	−6.03
3	9	7.84[e]	−24.5	5.10
4	8	0.313[e]	−22.3	17.3
4	9	−2.80[e]	−1.37	9.30
5	7	−3.75[e]	26.4	−16.5
5	8	−6.43[e]	0.842[c]	−3.75
5	9	2.02[e]	−83.0	44.4

[a] In [(kmol Å e)/kcal]. [b] In [kcal/{mol Å^2}]. [c] Parameters ϑ with $\Delta\vartheta(-E_j) = \Delta\vartheta(E_j)$. [d] In [kcal/{mol (10 deg)^2}]. [e] In [kcal/{mol Å (10 deg)}].

Appendix: PMM/O Parameters

Table 3 gives the nonzero off-diagonal force constants $\tilde{k}_{ij}(0)$ and the associated linear response parameters $\alpha_{ij,u}$, $u \in \{x, y\}$, of the optimized force field PMM/O (cf. Table 2).

Supporting Information Available: Table, figures, equations, and text explaining and discussing the Boltzmann-weighted conformations of isolated NMA, the mean field geometry of NMA in aqueous solution, and the reason why a nonredundant spectroscopic angular potential at an sp^2 hybridized center, which is defined in terms of two bond angles, is equivalent to a sum of three harmonic potentials defined by the three linearly dependent bond angles present at that center. This material is available free of charge via the Internet at http://pubs.acs.org.

References and Notes

(1) Byler, D. M.; Susi, H. *Biopolymers* **1986**, *25*, 469–487.
(2) Barth, A.; Zscherp, C. *Q. Rev. Biophys.* **2002**, *35*, 369–430.
(3) Siebert, F. *Methods Enzymol.* **1995**, *246*, 501–526.
(4) Krimm, S.; Bandekar, J. *Adv. Protein Chem.* **1986**, *38*, 181–364.
(5) Torii, H.; Tasumi, M. *J. Chem. Phys.* **1992**, *97*, 86–91.
(6) Torii, H.; Tasumi, M. *J. Chem. Phys.* **1992**, *97*, 92–98.
(7) Schultheis, V.; Reichold, R.; Schropp, B.; Tavan, P. *J. Phys. Chem. B* **2008**, *112*, 12217–12230.
(8) Ham, S.; Kim, J. H.; Lee, H.; Cho, M. H. *J. Chem. Phys.* **2003**, *118*, 3491–3498.
(9) Bour, P.; Keiderling, T. A. *J. Chem. Phys.* **2003**, *119*, 11253–11262.
(10) Lee, H.; Kim, S. S.; Choi, J. H.; Cho, M. *J. Phys. Chem. B* **2005**, *109*, 5331–5340.
(11) Gaigeot, M. P.; Vuilleumier, R.; Sprik, M.; Borgis, D. *J. Chem. Theory Comput.* **2005**, *1*, 772–789.
(12) Schmitz, M.; Tavan, P. On the art of computing the IR spectra of molecules in condensed phase. In *Modern methods for theoretical physical*

chemistry of biopolymers; Tanaka, S., Lewis, J., Eds.; Elsevier: Amsterdam, 2006; Chapter 8, pp 157−177.

(13) Zhuang, W.; Abramavicius, D.; Hayashi, T.; Mukamel, S. *J. Phys. Chem. B* **2006**, *110*, 3362–3374.

(14) Torii, H. *J. Phys. Chem. B* **2007**, *111*, 5434–5444.

(15) Ahlstrom, P.; Wallqvist, A.; Engstrom, S.; Jonsson, B. *Mol. Phys.* **1989**, *68*, 563–581.

(16) Harder, E.; Kim, B. C.; Friesner, R. A.; Berne, B. J. *J. Chem. Theory. Comput.* **2005**, *1*, 169–180.

(17) Guillot, B. *J. Mol. Liq.* **2002**, *101*, 219–260.

(18) Ponder, J. W.; Case, D. A. Force fields for protein simulations. In *Protein Simulations*; Academic Press Inc.: San Diego, 2003; Vol. 66.

(19) Tavan, P.; Carstens, H.; Mathias, G. Molecular dynamics simulations of proteins and peptides: Problems, achievements, and perspectives. In *Protein Folding Handbook*; Buchner, J., Kiefhaber, T., Eds.; Wiley-VCH: Weinheim, 2005; Vol. 1.

(20) Nonella, M.; Mathias, G.; Tavan, P. *J. Phys. Chem. A* **2003**, *107*, 8638–8647.

(21) Schmitz, M.; Tavan, P. *J. Chem. Phys.* **2004**, *121*, 12247–12258.

(22) Lifson, S.; Stern, P. S. *J. Chem. Phys.* **1982**, *77*, 4542–4550.

(23) Palmö, K.; Pietilä, L.-O.; Krimm, S. *J. Comput. Chem.* **1991**, *12*, 385–390.

(24) Palmö, K.; Mannfors, B.; Mirkin, N. G.; Krimm, S. *Biopolymers* **2003**, *68*, 383–394.

(25) Brooks, B. R.; Bruccoleri, R. E.; Olafson, B. D.; States, D. J.; Swaminathan, S.; Karplus, M. *J. Comput. Chem.* **1983**, *4*, 187–217.

(26) Pearlman, D.; Case, D.; Caldwell, J.; Ross, W.; Cheatham, T., III; DeBolt, S.; Ferguson, D.; Seibel, G.; Kollman, P. *Comput. Phys. Commun.* **1995**, *91*, 1–41.

(27) Scott, W. R. P.; Hünenberger, P. H.; Tironi, I. G.; Mark, A. E.; Billeter, S. R.; Fennen, J.; Torda, A. E.; Huber, T.; Krüger, P.; van Gunsteren, W. F. *J. Phys. Chem. A* **1999**, *103*, 3596–3607.

(28) Mathias, G.; Egwolf, B.; Nonella, M.; Tavan, P. *J. Chem. Phys.* **2003**, *118*, 10847–10860.

(29) *CPMD*, version 3.9; copyright IBM Corp. 1990−2008, copyright MPI für Festkörperforschung Stuttgart 1997−2001; see also www.cpmd.org.

(30) Becke, A. D. *Phys. Rev. A* **1988**, *38*, 3098–3100.

(31) Perdew, J. P.; Yue, W. *Phys. Rev. B* **1986**, *33*, 8800–8802.

(32) Troullier, N.; Martins, J. L. *Phys. Rev. B* **1991**, *43*, 1993–2005.

(33) Eichinger, M.; Tavan, P.; Hutter, J.; Parrinello, M. *J. Chem. Phys.* **1999**, *110*, 10452–10467.

(34) Schropp, B.; Tavan, P. *J. Phys. Chem. B* **2008**, *112*, 6233–6240.

(35) Mirkin, N. G.; Krimm, S. *J. Mol. Struct.: THEOCHEM* **1995**, *334* (17), 1–6.

(36) Mirkin, N. G.; Krimm, S. *J. Mol. Struct.* **1991**, *242* (39), 143–160.

(37) Press, W. H.; Teukolsky, S. A.; Vetterling, W. T.; Flannery, B. P. *Numerical Recipes in C: The Art of Scientific Computing*; Cambridge University Press: Cambridge, 1992.

(38) MacKerell, A. D.; Bashford, D.; Bellott, M.; Dunbrack, R. L.; Evanseck, J. D.; Field, M. J.; Fischer, S.; Gao, J.; Guo, H.; Ha, S.; Joseph-McCarthy, D.; Kuchnir, L.; Kuczera, K.; Lau, F. T. K.; Mattos, C.; Michnick, S.; Ngo, T.; Nguyen, D. T.; Prodhom, B.; Reiher, W. E.; Roux, B.; Schlenkrich, M.; Smith, J. C.; Stote, R.; Straub, J.; Watanabe, M.; Wiorkiewicz-Kuczera, J.; Yin, D.; Karplus, M. *J. Phys. Chem. B* **1998**, *102*, 3586–3616.

(39) Jorgensen, W. L.; Chandrasekhar, J.; Madura, J. D.; Impey, R. W.; Klein, M. L. *J. Chem. Phys.* **1983**, *79*, 926–935.

(40) Singh, U. C.; Kollman, P. A. *J. Comput. Chem.* **1984**, *5*, 129–145.

(41) Lumley Jones, R. *J. Mol. Spectrosc.* **1963**, *11*, 411–421.

(42) Mayne, L. C.; Hudson, B. *J. Phys. Chem.* **1991**, *95*, 2962–2967.

(43) Kubelka, J.; Keiderling, T. A. *J. Phys. Chem. A* **2001**, *105*, 10922–10928.

(44) Goldstein, H.; Poole, C. P., Jr.; Safko, J. L., Sr. *Klassische Mechanik*; Wiley-VCH: Berlin, 2006.

(45) Nikitin, A. M.; Lyubartsev, A. P. *J. Comput. Chem.* **2007**, *28*, 2020–2026.

(46) Berendsen, H. J. C.; Postma, J. P. M.; van Gunsteren, W. F.; DiNola, A.; Haak, J. R. *J. Chem. Phys.* **1984**, *81*, 3684–3690.

(47) Niedermeier, C.; Tavan, P. *J. Chem. Phys.* **1994**, *101*, 734–748.

(48) Niedermeier, C.; Tavan, P. *Mol. Simul.* **1996**, *17*, 57–66.

(49) Verlet, L. *Phys. Rev.* **1967**, *159*, 98–103.

(50) Lingenheil, M.; Denschlag, R.; Reichold, R.; Tavan, P. *J. Chem. Theory Comput.* **2008**, *4*, 1293–1306.

(51) Borysow, J.; Moraldi, M.; Frommhold, L. *J. Mol. Phys.* **1985**, *56*, 913–922.

(52) Schrader, T. Personal communication.

(53) Watanabe, K.; Klein, M. L. *Chem. Phys.* **1989**, *131*, 157–167.

(54) Patel, S.; Brooks, C. L., III. *J. Comput. Chem.* **2004**, *25*, 1–15.

JP101358R